HHS Public Access

Author manuscript

J Am Chem Soc. Author manuscript; available in PMC 2021 May 06.

Published in final edited form as:

J Am Chem Soc. 2020 May 06; 142(18): 8142–8146. doi:10.1021/jacs.0c01861.

Mimicking the Constrained Geometry of a Nitrogen-Fixation Intermediate

Tianchang Liu, **Michael R. Gau**, **Neil C. Tomson***

P. Roy and Diana T. Vagelos Laboratories, Department of Chemistry, University of Pennsylvania, 231 South 34th Street, Philadelphia, Pennsylvania, 19104, United States.

Abstract

Both biological and industrial nitrogen reduction catalysts activate N_2 at multinuclear binding sites with constrained Fe–Fe distances. This contrasts with molecular diiron systems, which routinely form linear N_2 bridges to minimize steric interactions. Model compounds that capture the salient geometric features of N_2 binding by the nitrogenase enzymes and Mittasch catalysts would contribute to understanding their high N_2-reduction activity. It is shown in the present study that use of a geometrically flexible, dinucleating macrocycle allows for the formation of a bridging N_2 ligand with an unusual Fe–Ct_{N2}–Fe angle of 150° (Ct_{N2} = centroid of N_2), a geometry that approximates the α-N_2 binding mode on Fe(111) surfaces that precedes N_2 bond cleavage. The cavity size the macrocycle prevents the formation of a linear Fe–N_2–Fe unit and leads to orbital interactions that are distinct from those available to the linear configuration.

Ammonia (NH_3) is produced annually on a ~180 megaton scale, largely to provide fixed nitrogen for plants.[1] The generally accepted mechanism by which industrial NH_3-synthesis catalysts bind and activate N_2 invokes multinuclear Fe sites, and recent advances in the understanding of biological N_2 fixation points to a similar need for multiple Fe centers at the site of N_2 binding. As such, the coordination chemistry of N_2 continues to be an area of interest as chemists attempt to adapt the superior performance of these ammonia synthesis catalysts into molecular systems.

Both biological and industrial catalysts constrain the geometries of their multinuclear, N_2-binding sites. Biological nitrogen fixation occurs at Fe_7MS_9C cofactors (M = Mo, V, Fe), found within the active sites of the nitrogenase enzymes.[2–4] While many potential sites of N_2 binding in these cofactors have been proposed,[5–7] recent work has focused on a “belt” position that spans two, low-coordinate Fe ions ($d_{Fe–Fe}$ = *ca.* 2.6 Å, Figure 1).[8–910–11] Industrial ammonia synthesis is also understood to use specific multi-iron centers to activate N_2.[12–13] The catalysts used in the Haber-Bosch process are typically based on metallic iron with main group promotors, the most active face of which is Fe(111).[14–15] Following initial physisorption through end-on N_2-binding (γ-N_2, Figure 1), the adsorbate moves into a

***Corresponding Author**: tomson@upenn.edu. Phone: +1 (215) 898-6208.

ASSOCIATED CONTENT

Supporting Information

Experimental section, NMR spectra, IR spectra, computational details (PDF), crystallographic data (CIF format). This material is available free of charge via the Internet at http://pubs.acs.org.

bridging, side-on binding mode (α-N_2) prior to N–N bond cleavage.[16–21] This binding mode (and the proposed α'-N_2 structure that follows[15,18]) is thought to be critical to N–N bond activation.

The geometry of the α-N_2 intermediate appears to be impacted by the constrained Fe–Fe distance of *ca.* 4.1 Å for top-layer Fe atoms, which leads to an estimate Fe–Ct_{N2}–Fe angle to *ca.* 130°. This contrasts with the vast majority of known molecular systems,[22] which form linear Fe–Ct_{N2}–Fe bridges to minimize steric repulsion. The development of molecular systems that can offer constrained, multiiron sites for N_2 binding is thus of interest for its potential to inform our understanding of industrial (and biological) N_2 fixation.

In this Communication, we describe the synthesis, characterization, and electronic structure of unique diiron-μ-N_2 complexes. The use of a dinucleating macrocycle constrains the geometry of the Fe–N_2–Fe unit, leading to orbital interactions that are unavailable to traditional, linear $Fe_2(\mu$-$N_2)$ complexes but are of interest for their potential to contribute to multinuclear N_2 bond cleavage. We use the $^3PDI_2$ macrocycle, which contains two pyridyldiimine groups connected by propylene linkers (Figure 2). This ligand was recently shown to stabilize a range of bimetallic systems with different core oxidation states and geometries.[23–25] This work involved the Fe–Fe bonded complexes illustrated at the top-left of Figure 2, [($^3PDI_2$)$Fe_2(\mu$-Cl)$(PR_3)_2$][OTf] (**^{R}[Fe$_2$Cl]$^+$**, R = Me, Ph), which provided a starting point for the present study.

We set out to explore the binding of N_2 to reduced forms of the **^{R}[Fe$_2$Cl]$^+$** complexes. Chemical reduction with 2.0 equiv of KC_8 under an atmosphere of N_2 resulted in color changes from dark brown to purplish red. After workup, the products ($^3PDI_2$)$Fe_2(\mu$-$N_2)$ $(PR_3)_2$ (**^{R}[Fe$_2$N$_2$]^0**, Figure 2) were isolated in moderate spectroscopic yields (*ca.* 50–60 %) and low yields on crystallization (11 % for R = Me and 35 % for R = Ph). Crystallographic analysis of both **^{R}[Fe$_2$N$_2$]^0** complexes revealed μ-N_2-κ^1(N),κ^1(N') units that bridge between the metal centers. The Fe–Ct_{N2}–Fe angles of 150.1° (R = Me) and 151.7° (R = Ph) are similar to the cyclic $M_2Fe_3(N_2)_3$ complexes described by Holland (see below) but significantly more acute than known dinuclear $Fe_2(\mu$-$N_2)$ complexes (Fe–Ct_{N2}–Fe > 165°). Three μ-N_2 complexes are known that contain (PDI)Fe units; all display linear Fe–Ct_{N2}–Fe angles (174.1–177.8°).[26–27] The N–N distance of 1.135(3) Å in **^{Me}[Fe$_2$N$_2$]^0** [1.139(4) Å in **^{Ph}[Fe$_2$N$_2$]^0**] shows mild activation compared to free dinitrogen (1.098 Å) and is similar to those observed in related (PDI)Fe–N_2 complexes (*ca.* 1.10–1.13 Å; see Supporting Information).[26–34]

Recent reports in the literature have highlighted the use of ligand design to support multinuclear iron systems that can activate N_2. These include Murray's use of a rigid, trinucleating cyclophane ligand that supports the iron-mediated reduction of N_2 into μ-NH_x groups (x = 1, 2; Figure 3).[35] Use of the same ligand scaffold with Cu led to a $Cu_3(\mu^3$-$N_2)$ species,[36] but a corresponding $Fe_3(N_2)$ species has yet to be detected. Holland and co-workers reported the first example of Fe-mediated N_2 cleavage into nitrides (Figure 3).[37] Extensive computational investigations identified a candidate for N_2 activation that was proposed to bind N_2 in a geometry that involves both end-on and side-on coordination modes.[38] In related chemistry, Holland described the cyclic $M_2Fe_3(N_2)_3$-containing

complexes (Figure 3; M = K, Rb, Cs),[39] which form bridging N_2 geometries that had only previously been found with a handful of early transition metals.[40–43] N_2 is weakly bound in these examples, and before the present case, it was unclear if the acute Fe–Ct_{N2}–Fe angles of *ca.* 150° can exist in the absence of the stabilizing alkali metal ions. Further, the extent to which this change in geometry impacts the Fe–N_2 bonding interaction is currently unknown, prompting us to examine the electronic structures of the ^{R}**[Fe$_2$N$_2$]^0** complexes and the factors that determine their unusual N_2-binding geometries.

Both compounds were found to be diamagnetic in solution, displaying C_{2v} symmetry, as determined by a characteristic 4:4:2:2 ratio of integrals for the features that result from the diastereotopic methylene groups. The retention of phosphine ligands was apparent from the $^{31}P\{^1H\}$ NMR spectra, which revealed singlets at 22.33 ppm for R = Me and 60.97 ppm for R = Ph (THF-d_8, 298 K). The N_2 unit was found to be kinetically inert with respect to dissociation. Either application of a dynamic vacuum or storage of the material under an atmosphere of Ar did not result in detectable decomposition. Both compounds display high N–N stretching frequencies: 2003 cm^{-1} for ^{Me}**[Fe$_2$N$_2$]^0** and 1959 cm^{-1} for ^{Ph}**[Fe$_2$N$_2$]^0**. The latter shifts to 1896 cm^{-1} ($\Delta\nu_{NN}$ = 63 cm^{-1}; *cf.* $\Delta\nu_{NN}$ would be 66 cm^{-1} assuming a simple oscillator) on use of $^{15}N_2$ during the synthesis, consistent with our assignment of this feature as resulting from an isolated, diatomic N–N stretching mode. Bridging N_2 complexes are typically IR inactive due to the inversion symmetry of linear M–N_2–M units. In this case, the out-of-plane positioning of the N_2 unit results in significant intensity in the IR spectrum for the N–N stretch. This positioning appears to result from constraints imposed by the macrocyclic ligands in ^{R}**[Fe$_2$N$_2$]^0**, which display an expanded, arch-shaped geometry compared to the more contracted ligand geometries in ^{R}**[Fe$_2$Cl]$^+$**. The angle between the planes of the pyridyl rings illustrates the difference between the structures, with ∠py-py = 89.7° for ^{Me}**[Fe$_2$N$_2$]^0** (82.2° for ^{Ph}**[Fe$_2$N$_2$]^0**) compared to 21.7° in ^{Me}**[Fe$_2$Cl]$^+$**. The expansion of the macrocycle appears to be limited, however, by torsion within the aliphatic linker (Figure 2). Further unfurling of the macrocycle would force the central methylene into the pocket between the iron centers.

We recently adapted the Δ parameter, an empirical metric used to describe the physical oxidation states of PDI ligands based on characteristic bond lengths of the ligand backbone,[44] into units suitable for $^3PDI_2$.[25] The Δ values for ^{R}**[Fe$_2$N$_2$]^0** (0.067 for ^{Ph}**[Fe$_2$N$_2$]^0**, 0.060 for ^{Me}**[Fe$_2$N$_2$]^0**) lie in a range most closely associated with a $(^3PDI_2)^{4-}$ electron distribution. Cyclic voltammetry on ^{Ph}**[Fe$_2$N$_2$]^0** revealed oxidations at −1.52 and −1.26 V, which likely correspond to PDI-based oxidations. No reduction features of comparable intensity were observed out to the limits of the electrochemical window for the solvent (THF, see Supporting Information). Together with the diamagnetism of the complex and the apparent equivalence of the coordination spheres about the two metal centers, the Δ values suggest the presence of either two low-spin Fe^{II} ions or two intermediate-/high-spin ions that are strongly antiferromagnetically coupled. We can immediately discount the high-spin assignment due to the short Fe–N_{PDI} and Fe–P distances (see Supporting Information). DFT calculations were used for further analysis of the electronic structure.

Optimization of a truncated form of ^{Me}**[Fe$_2$N$_2$]^0** provided excellent agreement with the experimental data (see Supporting Information), including a Fe–Ct_{N2}–Fe angle of 149.7°, an

N–N bond length of 1.148 Å, and ν_{NN} = 2010 cm^{-1} ($\Delta\nu_{NN}$ = 67 cm^{-1}). The experimental Δ value that led to the $(^3PDI_2)^{4-}$ oxidation state assignment was also reproduced computationally (Δ_{calc} = 0.064). The **^{R}[Fe$_2$N$_2$]^0** complexes formally contain d^8, Fe^0 metal centers, but the low-energy π* manifold of the PDI fragment is well known to accept electron density in lieu of $Fe^{<II}$ oxidation states.[28, 31, 45] Consistent with the oxidation state assignments inferred from the crystallographic bond lengths, the metal centers are best described as Fe^{II}. The Fe^{II} ions further appear to be in low-spin electron configurations. The d_π manifold (*xz*±*xz*, *yz*±*yz*, *xy*±*xy*) was found to be fully occupied, with typical π-backbonding interactions between out-of-phase d_π fragment orbitals combinations (*xy*–*xy*, *yz*–*yz*) and the N_2 π* manifold. Doing so yields the HOMO-6 [(*yz*–*yz*) + π^*_z)] and HOMO-7 [(*xy*–*xy*) + π^*_x)] (Figure 4; for a quantitative MO diagram, see Figure S23 in the Supporting Information).

For mononuclear (PDI)Fe complexes, the presence of two electron's worth of electron density on the ligand typically results from single occupation of both redox-active orbitals (b_1 and a_2).[25, 45] In the case of **^{R}[Fe$_2$N$_2$]^0**, however, the filled, in-phase (HOMO) and out-of-phase (HOMO-1, Figure 4) combinations [(b_1+z^2)±(b_1+z^2)] are primarily responsible for the four electron reduction of $^3PDI_2$.

Interestingly, the (b_1+z^2) fragment would normally be non-bonding with respect to the N_2 π* manifold, but HOMO-1 reveals a bonding interaction between π^*_z and [(b_1+z^2)–(b_1+z^2)]. Thus, it appears that the constrained geometry imposed by the macrocycle allows for an additional interaction between the Fe-*d* and N_2-π* manifolds compared to linear Fe–N_2–Fe motifs. The extent of mixing is too low in the present case to result in a significant increase in the degree of N_2 activation, but it is noteworthy that this type of interaction repeats in LUMO+4 (Figure 4), which results from mixing of π^*_z with an out-of-phase combination of x^2-y^2. Complexes with weaker ligand field donor sets, in conjunction with constrained Fe–Ct_{N2}–Fe angles, may be able to take advantage of these orbital interactions for N_2 bond cleavage.

The importance of constrained-geometry multinuclear iron sites for N_2 binding and activation repeat throughout biological and heterogeneous catalysts, but few molecular systems are available that can mimic these interactions. This report described the dinuclear binding of N_2 in a coordination environment reminiscent of the α-N_2 binding mode to Fe(111). The use of a macrocycle with flexible alkyl linkers allowed the metal centers to separate in space following reduction of an Fe–Fe bonded starting material, providing a location for N_2 binding. However, the limited size of the macrocycle cavity prevented the Fe_2N_2 unit from adopting a linear linkage, as is common in diiron μ-N_2 chemistry. The orbital interactions made possible by this geometry provide an avenue for facilitating N_2 reduction, thereby highlighting the manner in which geometric tuning of the active site constitutes an important factor in catalytic ammonia synthesis.

Supplementary Material

Refer to Web version on PubMed Central for supplementary material.

ACKNOWLEDGMENT

We thank the donors of the American Chemical Society Petroleum Research Fund (57346-DNI3), the National Institutes of Health (R35GM128794), and the University of Pennsylvania for support of this research. The NIH supplemental awards 3R01GM118510-03S1 and 3R01GM087605-06S1 as well as the Vagelos Institute for Energy Science and Technology supported the purchase of the NMR instrumentation used in this study.

Funding Sources

No competing financial interests have been declared.

REFERENCES

1. U.S. Geological Survey, Mineral commodity summaries 2020: U.S. Geological Survey, 2020, 200 p., 10.3133/mcs2020.
2. Eady RR, Structure−Function Relationships of Alternative Nitrogenases. Chem. Rev 1996, 96 (7), 3013–3030. [PubMed: 11848850]
3. Burgess BK; Lowe DJ, Mechanism of Molybdenum Nitrogenase. Chem. Rev 1996, 96 (7), 2983–3012. [PubMed: 11848849]
4. Sippel D; Einsle O, The structure of vanadium nitrogenase reveals an unusual bridging ligand. Nat. Chem. Bio 2017, 13 (9), 956–960. [PubMed: 28692069]
5. Schimpl J; Petrilli HM; Blöchl PE, Nitrogen Binding to the FeMo-Cofactor of Nitrogenase. J. Am. Chem. Soc 2003, 125 (51), 15772–15778. [PubMed: 14677967]
6. Thorhallsson AT; Benediktsson B; Bjornsson R, A model for dinitrogen binding in the E4 state of nitrogenase. Chem. Sci 2019, 10 (48), 11110–11124. [PubMed: 32206260]
7. Hoffman BM; Lukoyanov D; Yang Z-Y; Dean DR; Seefeldt LC, Mechanism of Nitrogen Fixation by Nitrogenase: The Next Stage. Chem. Rev 2014, 114 (8), 4041–4062. [PubMed: 24467365]
8. Dance I, How feasible is the reversible S-dissociation mechanism for the activation of FeMo-co, the catalytic site of nitrogenase? Dalton Trans. 2019, 48 (4), 1251–1262. [PubMed: 30607401]
9. Speelman AL; Čorić I; Van Stappen C; DeBeer S; Mercado BQ; Holland PL, Nitrogenase-Relevant Reactivity of a Synthetic Iron–Sulfur–Carbon Site. J. Am. Chem. Soc 2019, 141 (33), 13148–13157. [PubMed: 31403298]
10. Spatzal T; Perez KA; Einsle O; Howard JB; Rees DC, Ligand binding to the FeMo-cofactor: Structures of CO-bound and reactivated nitrogenase. Science 2014, 345 (6204), 1620. [PubMed: 25258081]
11. Sippel D; Rohde M; Netzer J; Trncik C; Gies J; Grunau K; Djurdjevic I; Decamps L; Andrade SLA; Einsle O, A bound reaction intermediate sheds light on the mechanism of nitrogenase. Science 2018, 359 (6383), 1484. [PubMed: 29599235]
12. Ertl G, Elementary Steps in Ammonia Synthesis In Catalytic Ammonia Synthesis: Fundamentals and Practice; Jennings JR, Ed.; Springer US: Boston, 1991; 116–120.
13. Freund H-J; Kuhlenbeck H, Chapter 10 - Adsorption on Metals In Handbook of Surface Science; Horn K; Scheffler M, Eds.; Elsevier: Amsterdam, 2000; 2, 715–718.
14. Spencer ND; Schoonmaker RC; Somorjai GA, Iron single crystals as ammonia synthesis catalysts: Effect of surface structure on catalyst activity. J. Catal 1982, 74 (1), 129–135.
15. Bozso F; Ertl G; Grunze M; Weiss M, Interaction of nitrogen with iron surfaces: I. Fe(100) and Fe(111). J. Catal 1977, 49 (1), 18–41.
16. Qian J; An Q; Fortunelli A; Nielsen RJ; Goddard WA, Reaction Mechanism and Kinetics for Ammonia Synthesis on the Fe(111) Surface. J. Am. Chem. Soc 2018, 140 (20), 6288–6297. [PubMed: 29701965]
17. Ertl G; Lee SB; Weiss M, Kinetics of nitrogen adsorption on Fe(111). Surf. Sci 1982, 114 (2), 515–526.
18. Grunze M; Strasser G; Golze M, Precursor mediated and direct adsorption of molecular nitrogen on Fe{111}. Appl. Phys. A-Mater 1987, 44, 19–29.

19. Mortensen JJ; Hansen LB; Hammer B; Nørskov JK, Nitrogen Adsorption and Dissociation on Fe(111). J. Catal 1999, 182 (2), 479–488.
20. Christoffersen E; Mortensen J-J; Stoltze P; Nørskov JK, N_2 Interaction with Fe Surfaces. Isr. J. Chem 1998, 38 (4), 279–284.
21. Hammer B; Nørskov JK, Theoretical surface science and catalysis—calculations and concepts In Advances in Catalysis, Academic Press: 2000; Vol. 45, pp 71–129.
22. Burford RJ; Fryzuk MD, Examining the relationship between coordination mode and reactivity of dinitrogen. Nat. Chem. Rev 2017, 1 (4), 0026.
23. Cui P; Wang Q; McCollom SP; Manor BC; Carroll PJ; Tomson NC, Ring-Size-Modulated Reactivity of Putative Dicobalt-Bridging Nitrides: C−H Activation versus Phosphinimide Formation. Angew. Chem. Int. Ed 2017, 56 (50), 15979–15983.
24. Zhang S; Wang Q; Thierer LM; Weberg AB; Gau MR; Carroll PJ; Tomson NC, Tuning Metal–Metal Interactions through Reversible Ligand Folding in a Series of Dinuclear Iron Complexes. Inorg. Chem 2019, 58 (18), 12234–12244. [PubMed: 31448589]
25. Wang Q; Zhang S; Cui P; Weberg AB; Thierer LM; Manor BC; Gau MR; Carroll PJ; Tomson NC, Interdependent Metal–Metal Bonding and Ligand Redox-Activity in a Series of Dinuclear Macrocyclic Complexes of Iron, Cobalt, and Nickel. Inorg. Chem 2019, doi: 10.1021/acs.inorgchem.9b02339.
26. Russell SK; Darmon JM; Lobkovsky E; Chirik PJ, Synthesis of Aryl-Substituted Bis(imino)pyridine Iron Dinitrogen Complexes. Inorg. Chem 2010, 49 (6), 2782–2792. [PubMed: 20143847]
27. Hojilla Atienza CC; Tondreau AM; Weller KJ; Lewis KM; Cruse RW; Nye SA; Boyer JL; Delis JGP; Chirik PJ, High-Selectivity Bis(imino)pyridine Iron Catalysts for the Hydrosilylation of 1,2,4-Trivinylcyclohexane. ACS Catal. 2012, 2 (10), 2169–2172.
28. Stieber SCE; Milsmann C; Hoyt JM; Turner ZR; Finkelstein KD; Wieghardt K; DeBeer S; Chirik PJ, Bis(imino)pyridine Iron Dinitrogen Compounds Revisited: Differences in Electronic Structure Between Four- and Five-Coordinate Derivatives. Inorg. Chem 2012, 51 (6), 3770–3785. [PubMed: 22394054]
29. Bart SC; Lobkovsky E; Chirik PJ, Preparation and Molecular and Electronic Structures of Iron(0) Dinitrogen and Silane Complexes and Their Application to Catalytic Hydrogenation and Hydrosilation. J. Am. Chem. Soc 2004, 126 (42), 13794–13807. [PubMed: 15493939]
30. Archer AM; Bouwkamp MW; Cortez M-P; Lobkovsky E; Chirik PJ, Arene Coordination in Bis(imino)pyridine Iron Complexes: Identification of Catalyst Deactivation Pathways in Iron-Catalyzed Hydrogenation and Hydrosilation. Organometallics 2006, 25 (18), 4269–4278.
31. Bart SC; Lobkovsky E; Bill E; Wieghardt K; Chirik PJ, Neutral-Ligand Complexes of Bis(imino)pyridine Iron: Synthesis, Structure, and Spectroscopy. Inorg. Chem 2007, 46 (17), 7055–7063. [PubMed: 17655227]
32. Darmon JM; Turner ZR; Lobkovsky E; Chirik PJ, Electronic Effects in 4-Substituted Bis(imino)pyridines and the Corresponding Reduced Iron Compounds. Organometallics 2012, 31 (6), 2275–2285. [PubMed: 22675236]
33. Fernández I; Trovitch RJ; Lobkovsky E; Chirik PJ, Synthesis of Bis(imino)pyridine Iron Di- and Monoalkyl Complexes: Stability Differences between FeCH2SiMe3 and FeCH2CMe3 Derivatives. Organometallics 2008, 27 (1), 109–118.
34. Tondreau AM; Milsmann C; Patrick AD; Hoyt HM; Lobkovsky E; Wieghardt K; Chirik PJ, Synthesis and Electronic Structure of Cationic, Neutral, and Anionic Bis(imino)pyridine Iron Alkyl Complexes: Evaluation of Redox Activity in Single-Component Ethylene Polymerization Catalysts. J. Am. Chem. Soc 2010, 132 (42), 15046–15059. [PubMed: 20882992]
35. Lee Y; Sloane FT; Blondin G; Abboud KA; García-Serres R; Murray LJ, Dinitrogen Activation Upon Reduction of a Triiron(II) Complex. Angew. Chem. Int. Ed 2015, 54 (5), 1499–1503.
36. Murray LJ; Weare WW; Shearer J; Mitchell AD; Abboud KA, Isolation of a (Dinitrogen)Tricopper(I) Complex. J. Am. Chem. Soc 2014, 136 (39), 13502–13505. [PubMed: 25238198]

37. Rodriguez MM; Bill E; Brennessel WW; Holland PL, N_2 Reduction and Hydrogenation to Ammonia by a Molecular Iron-Potassium Complex. Science 2011, 334 (6057), 780. [PubMed: 22076372]

38. Figg TM; Holland PL; Cundari TR, Cooperativity Between Low-Valent Iron and Potassium Promoters in Dinitrogen Fixation. Inorg. Chem 2012, 51 (14), 7546–7550. [PubMed: 22734966]

39. Grubel K; Brennessel WW; Mercado BQ; Holland PL, Alkali Metal Control over N–N Cleavage in Iron Complexes. J. Am. Chem. Soc 2014, 136 (48), 16807–16816. [PubMed: 25412468]

40. Hung Y-T; Yap GPA; Theopold KH, Unexpected reactions of chromium hydrides with a diazoalkane. Polyhedron 2019, 157, 381–388.

41. Vidyaratne I; Scott J; Gambarotta S; Budzelaar PHM, Dinitrogen Activation, Partial Reduction, and Formation of Coordinated Imide Promoted by a Chromium Diiminepyridine Complex. Inorg. Chem 2007, 46 (17), 7040–7049. [PubMed: 17649991]

42. Vidyaratne I; Gambarotta S; Korobkov I; Budzelaar PHM, Dinitrogen Partial Reduction by Formally Zero- and Divalent Vanadium Complexes Supported by the Bis-iminopyridine System. Inorg. Chem 2005, 44 (5), 1187–1189. [PubMed: 15732953]

43. Pun D; Lobkovsky E; Chirik PJ, Indenyl Zirconium Dinitrogen Chemistry: N_2 Coordination to an Isolated Zirconium Sandwich and Synthesis of Side-on, End-on Dinitrogen Compounds. J. Am. Chem. Soc 2008, 130 (18), 6047–6054. [PubMed: 18399632]

44. Römelt C; Weyhermüller T; Wieghardt K, Structural characteristics of redox-active pyridine-1,6-diimine complexes: Electronic structures and ligand oxidation levels. Coord. Chem. Rev 2019, 380, 287–317.

45. Bart SC; Chłopek K; Bill E; Bouwkamp MW; Lobkovsky E; Neese F; Wieghardt K; Chirik PJ, Electronic Structure of Bis(imino)pyridine Iron Dichloride, Monochloride, and Neutral Ligand Complexes: A Combined Structural, Spectroscopic, and Computational Study. J. Am. Chem. Soc 2006, 128 (42), 13901–13912. [PubMed: 17044718]

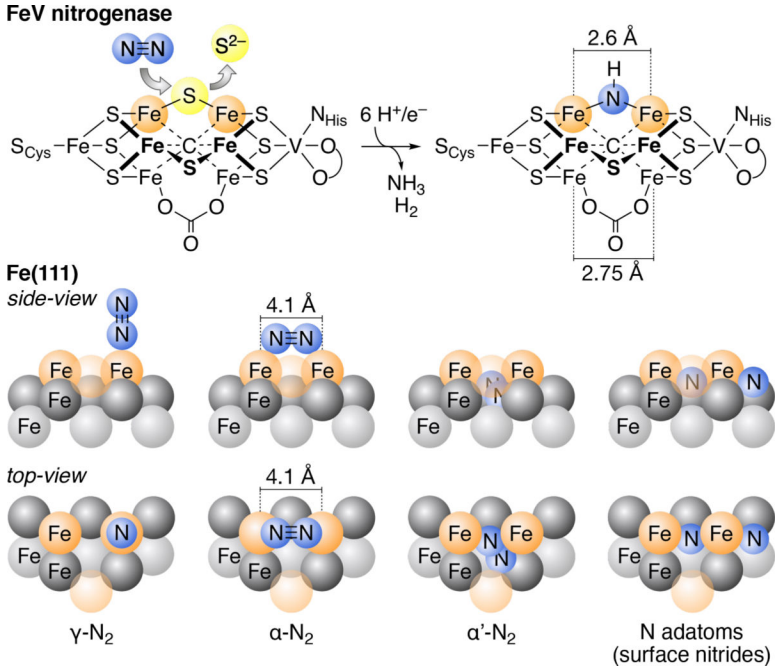

Figure 1.

Top: Proposed location of N_2 activation at the FeV cofactors. *Bottom*: Side- and top-views of the binding modes that precede rate-limiting formation of μ-nitrides on Fe(111) surfaces. The top-, second-, and third-layers of Fe are depicted with orange, dark grey, and light grey spheres, respectively.

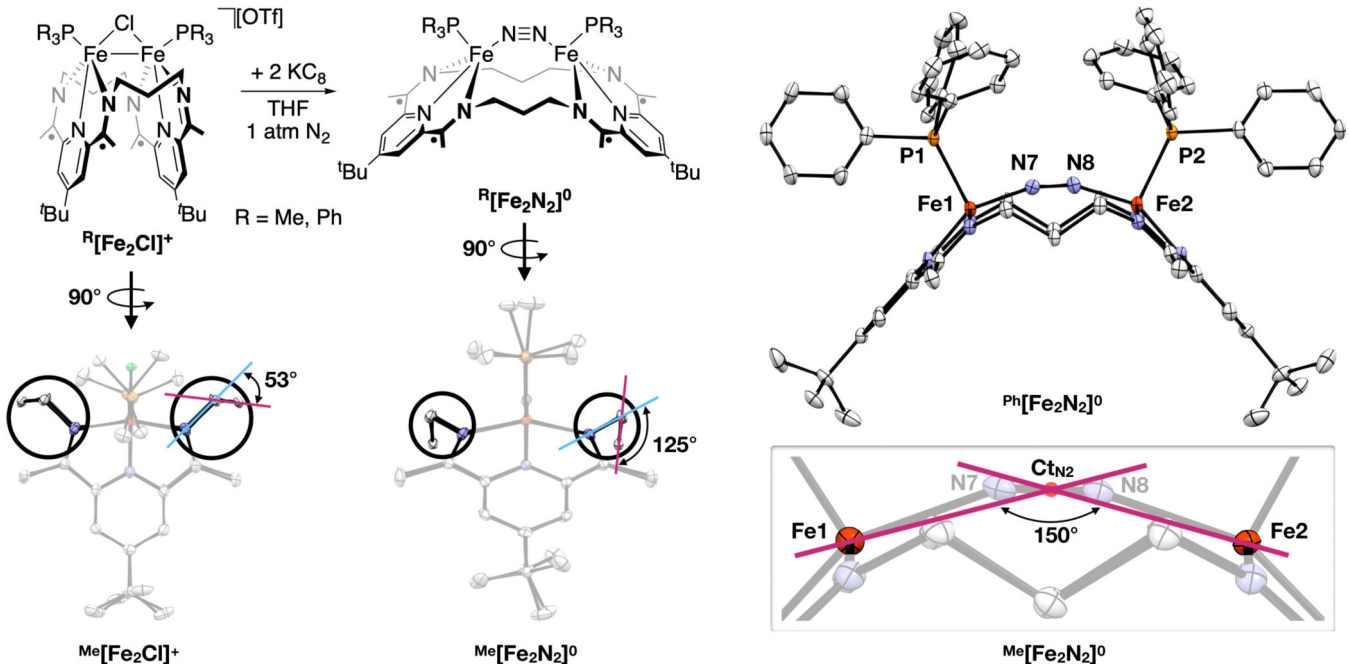

Figure 2.

Top-left: Synthetic scheme for the formation of $^{R}[Fe_2N_2]^0$. *Right*: Crystal structure of $^{Ph}[Fe_2N_2]^0$ and illustration of the acute Fe–Ct_{N2}–Fe angle exhibited by this series of complexes. *Bottom-left*: View along the Fe–Fe vectors for $^{Me}[Fe_2Cl]^+$ and $^{Me}[Fe_2N_2]^0$, highlighting the change in the angle between *i*) a plane created by the imino nitrogens and the linker-carbons α to the imino nitrogens (N– C_α–C_α–N) and *ii*) a plane created by the three linker carbons (C_α–C_β–C_α).

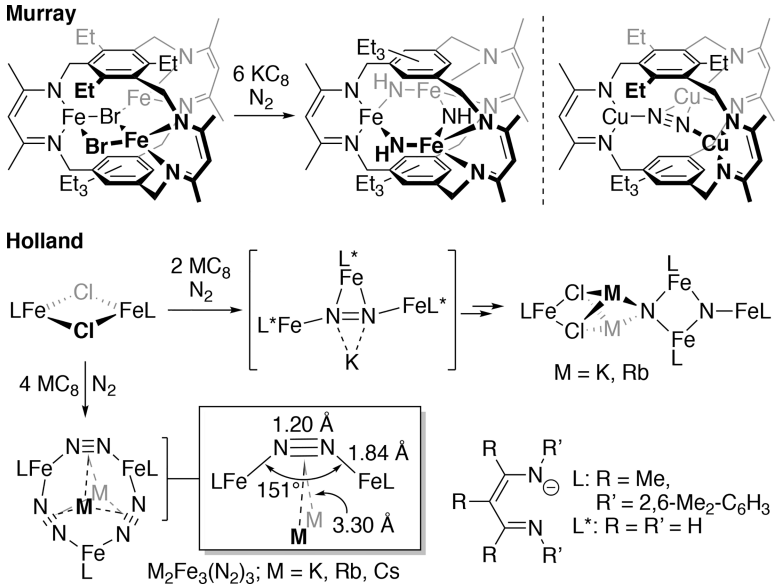

Figure 3.

Top-left, Middle: Multinuclear iron systems used for N_2 bond cleavage. *Top-right*: N_2-binding by a tricopper cyclophane complex. *Bottom*: Use of an M_2Fe_2 unit to bind N_2 with an acute Fe–Ct_{N2}–Fe angle.

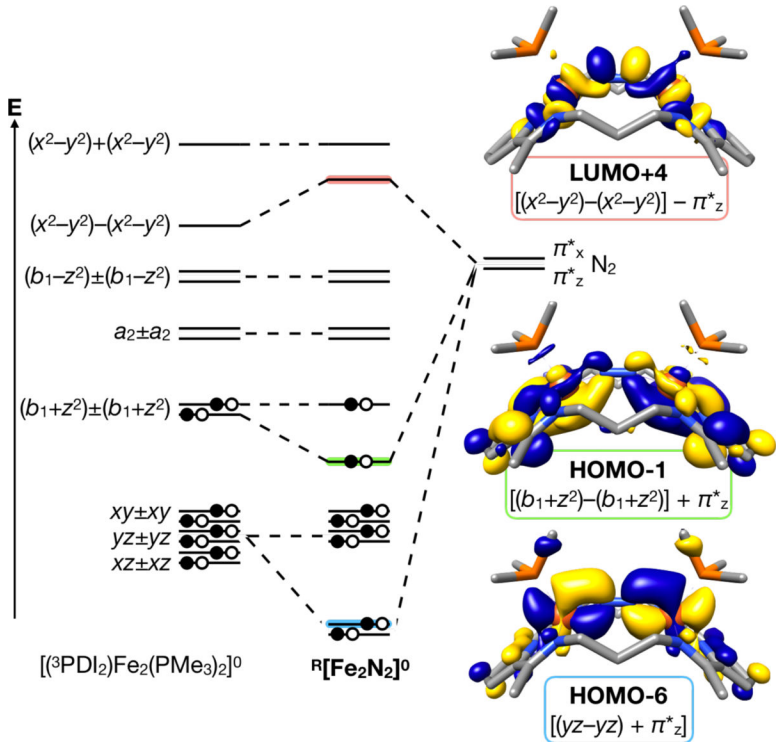

Figure 4.

Qualitative molecular orbital interaction diagram describing the admixture of the **π*** system of N_2 to the *d*-manifold within $^{Me}[Fe_2N_2]^0$.